CHINA COMMUNICATIONS

Bit-Interleaved Polar Coded Modulation with Iterative Successive Cancellation List Decoding

Hang Mu[1], Zheng Ma[2], George K. Karagiannidis[3], Panagiotis D. Diamantoulakis[3]

[1] The 10th Research Institute of China Electronics Technology Group Corporation, Chengdu 610036, Sichuan, China.
[2] the School of Information Science and Technology, Southwest Jiaotong University, Chengdu 610036, Sichuan, China.
[3] the Departmentof Electrical and Computer Engineering, Aristotle University of Thessaloniki, Thessaloniki 54 124, Greece.
[*] The corresponding author, email: muhang@my.swjtu.edu.cn

Abstract: This paper introduces bit-interleaved polar coded modulation with iterative detection/decoding (BIPCM-ID). In order to enable the soft output of successive cancellation list (SCL) decoding, two types of re-encoders are proposed, namely the max-re-encoder and min-re-encoder, respectively. Regarding the iterative decoding, we analytically verify that the average mutual information (AMI) between the transmitted and decoded symbols can approach the Shannon bound with the proposed schemes. Moreover, bit error rate (BER) and block error rate (BLER) in single-user and multi-user scenarios are studied. Finally, simulation results show that the performance of BIPCM-ID outperforms other bit-interleaved coded modulation (BICM) systems with LDPC and Turbo codes, while also reducing the computational complexity.

Keywords: BIPCM-ID; Polar code; SCMA; Re-encoder; SCL; AMI

I. INTRODUCTION

Recently, polar codes have been chosen as the coding scheme for the enhanced mobile broadband (eMBB) control channel of the 5th generation (5G) mobile networks. The capacity-achieving polar coding is an attractive forward errorcontrol solution for future wireless communication systems [1]. However, it requires long codeword length to achieve the capacity over a noisy channel. In the scenarios of 5G, the codeword lengths of polar codes are restricted to be no longer than 1024-bit with non-binary modulation, which degrades the BER and BLER performances. In fact, the degradations are mainly resulted from the inadequate polarization of subchannels and the choice of the labeling in polar coded modulation schemes [2].

In addition, the high-connectivity and high-capacity requirements of 5G in massive machine type communications (mMTC) inspire the non-orthogonal multiple access (NOMA) for multi-user utilization. As a promising technique of NOMA, sparse code multiple access (SCMA) is encouraged to combine with polar codes for the high spectral efficiency and low latency [3, 4]. Hence, the trade-off between the performance and the capacity of polar coded communications that comply with the requirements of 5G [5] becomes the main challenge of the receiver design. Nevertheless, the receiver's computational complexity also plays an important role in low-latency communications, which should be carefully considered.

1.1 Motivation and State-of-the-Art

Bit-interleaved coded modulation (BICM) [6, 7] with iterative decoding (BICM-ID) [8] is helpful to approach the capacity and obtainvery low BER at high SNR region. The bit-interleaved polar coded modulation (BIPCM) systems were presented in [9–11]. In [9] and [10], the authors investigated the modulation after polar encoding, and focused on the "mapping" of codewords to the 2^q-ary symbols, where the codeword

Received: Dec. 30, 2020
Revised: Jul. 11, 2021
Editor: Da Chen

length was not divisible by q. The authors in [11] considered the BICM system as a multi-channel model, where they constructed a unified compound polar code by taking advantages of the recursive structure of polar coding. However, the above strategies failed to realize the BIPCM-ID, mainly because of the absence of the soft information after decoding. In fact, the original successive cancellation (SC) decoder and successive cancellation list (SCL) decoder in [1], [12, 13] are not able to generate soft information of the codewords themselves.

In order to get the soft information, belief propagation (BP) decoder [14] and its modifications were proposed [15–17]. The soft cancellation (SCAN) decoder in [17] is considered as a modification of BP [18]. BP with flooding schedule suffers high complexity and memory requirements, but has excellent throughput. BP with SCAN schedule is low-complexity and memory efficient, but suffers from serial manners of the update of the soft information. However, the BER improvement can still be achieved by the iterative decoding, according to which, BIPCM-ID is directly realized by the BP and SCAN decoder in [19–21].

Concatenated code and hard-decision mechanism are adopted into the iterative decoding of polar codes. By using parity-check-aided decoder, the authors in [22] concatenated low-density parity-check (LDPC) code with polar code to obtain the soft information. In [23], a hard-decision feedback framework, termed as joint successive cancellation (JSC) decoding, was proposed. Some other advanced strategies are used for soft decoding of the polar codes [24–26], which make polar codes more powerful.

As it becomes evident from the above, the soft-in soft-out (SISO) SCL decoder for iterative decoding of polar code is still an attractive area to research. Furthermore, the analyses of mutual information (MI) and computational complexity of BIPCM-ID system are rare in literatures, which are the main motivations of this work.

1.2 Contributions

In this paper, we propose a novel BIPCM-ID, which is based on the design of a SISO SCL decoder. The SISO SCL decoder is enabled to output soft information of the codeword by using the re-encoder. The re-encoder inherits the simple coding structure of the original polar encoder and is modified according to the max-log and min-sum algorithms, in order to further decrease the computational complexity of calculating log-likelihood ratios (LLRs). The proposed BIPCM-ID is investigated in single-user and multi-user scenarios, where SCMA is employed to provide multi-user access. More specifically, the contributions in this work can be summarized as follows:

(1) We propose a novel BIPCM-ID, which complies with the requirements of codeword lengths of 5G eMBB control channel. To this direction, we introduce a soft feedback mechanism based on SCL decoder for polar code.

(2) The mutual information between the transmitted and decoded symbols is investigated for the proposed BIPCM-ID. The average mutual information (AMI) is verified to be able of approaching the Shannon bound under the given configurations in multi-user scenario.

(3) A comprehensive comparison of decoding computational complexities is made by simulations, which includes the proposed iterative SCL decoder and other soft output decoders, such as LDPC and Turbo decoders. It is shown that, the proposed iterative SCL decoder is capable of reducing both BER and BLER with acceptable computational complexity.

1.3 Structure

The rest of the paper is organized as follows. Section II describes the BIPCM-ID for single-user scenario, where SC and SCL decoders are reviewed. In section III, the original re-encoding algorithm and two types of modified re-encoders are introduced. Then, in section IV, the BIPCM-ID for multi-user scenario is presented, where the comparison of AMI between the BIPCM-ID and the LDPC coded BICM-ID in multi-user scenario is given. In section V, BER and BLER performances of the proposed BIPCM-ID system are presented. After that, the comparison of different coding schemes in terms of computational complexity is shown. Finally, conclusions are made in section VI.

II. SINGLE-USER MODEL AND PRELIMINARIES

The single-user polar coded system is based on the typical BICM-ID system, where the transmitter and receiver are shown in figure 1 and figure 2, respec-

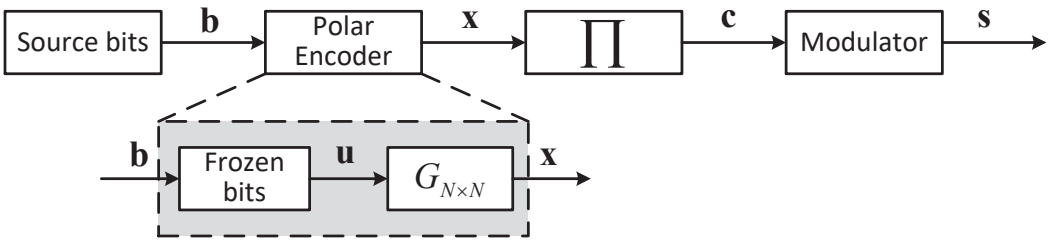

Figure 1. *Transmitter block diagram of single-user.*

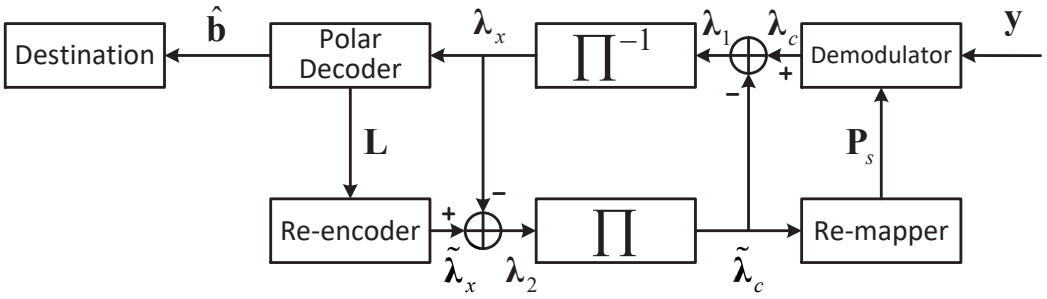

Figure 2. *Receiver block diagram of single-user.*

tively. Here, $\mathcal{A}$ and $\mathcal{A}^c$ denote the indices sets of information bits and frozen bits respectively, and vector $\mathbf{a} = [a_1, a_2, \ldots, a_n]$ is denoted as a_1^n.

At the transmitter, the user generates k information bits $\mathbf{b} = b_1^k$, while $\mathbf{b}$ is then encoded as the polar codewords $\mathbf{x} = x_1^N$ by polar encoder, where frozen bits are inserted according to $\mathcal{A}^c$.

Note that, after the channel polarization, the k most reliable sub-channels are chosen to carry the information bits, where $k = |\mathcal{A}|$, $|\cdot|$ denotes the cardinality, such that the code rate is $R = k/N$.

The interleaved codewords, $\mathbf{c} = c_1^N$, $\mathbf{c} = \Pi(\mathbf{x})$, are fed into the modulator to produce N_s symbols, $\mathbf{s} = s_1^{N_s}$, where $s_i \in \mathfrak{M}$, with $\mathfrak{M}$ being the constellation, $N_s = N/m$, $m = \log_2 |\mathfrak{M}|$.

Then, the modulated symbols are sent through an AWGN channel and are influenced by the complex Gaussian noises, $\mathbf{n} = n_1^{N_s}$, $n_i \sim \mathcal{CN}(0, N_0)$, where $i = 1, 2, \ldots, N_s$, N_0 is the noise power. Thus, the receiving model can be written as

$$\mathbf{y} = \mathbf{s} + \mathbf{n}. \tag{1}$$

At the receiver, the received signals $\mathbf{y} = y_1^{N_s}$ are sent into the MAP detector, where the bit-level LLRs $\lambda_{c_1}^N$ are calculated. In order to realize the BIPCM-ID, the bit-level LLR of the i-th bit of l-th symbol $\lambda_{c_{l,i}}$ is decomposed into extrinsic and intrinsic information, which can be expressed as

$$\lambda_{1_{l,i}} = \lambda_{c_{l,i}} - \tilde{\lambda}_{c_{l,i}}, \tag{2}$$

where, $\lambda_{1_{l,i}}$ and $\tilde{\lambda}_{c_{l,i}}$ indicate the extrinsic information and the intrinsic information, and are given by

$$\lambda_{1_{l,i}} = \log \frac{\sum_{s_l^+ \in \mathfrak{M}, s_l^+ : c_{l,i}=0} P(y_l|s_l^+) \cdot \prod_{j=1, j\neq i}^{m} P(c_{l,j})}{\sum_{s_l^- \in \mathfrak{M}, s_l^- : c_{l,i}=1} P(y_l|s_l^-) \cdot \prod_{j=1, j\neq i}^{m} P(c_{l,j})}, \tag{3}$$

and

$$\tilde{\lambda}_{c_{l,i}} = \log \frac{P(c_{l,i}=0)}{P(c_{l,i}=1)}, \tag{4}$$

where $P(\cdot)$ denotes probability, s_l^+ and s_l^- indicate the l-th symbols and their i-th labeling bits $c_{l,i}$ equal to 0 and 1 respectively, $P(c_{l,i})$ is the *priori* information.

The de-interleaver recovers the order of extrinsic information as $\lambda_{x_1}^N = \Pi^{-1}(\lambda_{1_1}^N)$ and feeds $\lambda_{x_1}^N$ into the decoder.

2.1 SC Decoding

The SC decoding is explicitly described in [1], the LLR of i-th decoded codeword can be written as

$$L_N^{(i)}(\lambda_{x_1}^N, \hat{u}_1^{i-1}|u_i) = \log \frac{P_N^{(i)}(\lambda_{x_1}^N, \hat{u}_1^{i-1}|u_i = 0)}{P_N^{(i)}(\lambda_{x_1}^N, \hat{u}_1^{i-1}|u_i = 1)}. \tag{5}$$

Both the numerator and denominator in the logarithm can be recursively computed depending on the parity of the indices of the polarized sub-channel, which are

$$\begin{aligned} &P_N^{(2i-1)}(\lambda_{x_1}^N, \hat{u}_1^{2i-2}|u_{2i-1}) \\ &= \sum_{u_{2i}} \frac{1}{2} P_{N/2}^{(i)}(\lambda_{x_1}^{N/2}, \hat{u}_{1,o}^{2i-2} \oplus \hat{u}_{1,e}^{2i-2}|u_{2i-1} \oplus u_{2i}), \\ &\qquad \cdot P_{N/2}^{(i)}(\lambda_{x_{N/2+1}}^N, \hat{u}_{1,e}^{2i-2}|u_{2i}) \end{aligned} \tag{6}$$

and

$$\begin{aligned} &P_N^{(2i)}(\lambda_{x_1}^N, \hat{u}_1^{2i-1}|u_{2i}) \\ &= \frac{1}{2} P_{N/2}^{(i)}(\lambda_{x_1}^{N/2}, \hat{u}_{1,o}^{2i-2} \oplus \hat{u}_{1,e}^{2i-2}|u_{2i-1} \oplus u_{2i}) \\ &\qquad \cdot P_{N/2}^{(i)}(\lambda_{x_{N/2+1}}^N, \hat{u}_{1,e}^{2i-2}|u_{2i}). \end{aligned} \tag{7}$$

Correspondingly, the LLR recursions can be expressed as

$$\begin{aligned} &L_N^{(2i-1)}(\lambda_{x_1}^N, \hat{u}_1^{2i-2}) = \\ &f\left(L_{N/2}^{(i)}(\lambda_{x_1}^{N/2}, \hat{u}_{1,o}^{2i-2} \oplus \hat{u}_{1,e}^{2i-2}), L_{N/2}^{(i)}(\lambda_{x_{N/2+1}}^N, \hat{u}_{1,e}^{2i-2})\right) \end{aligned} \tag{8}$$

and

$$\begin{aligned} L_N^{(2i)}(\lambda_{x_1}^N, \hat{u}_1^{2i-1}) = g\Big(&L_{N/2}^{(i)}(\lambda_{x_1}^{N/2}, \hat{u}_{1,o}^{2i-2} \oplus \hat{u}_{1,e}^{2i-2}), \\ &L_{N/2}^{(i)}(\lambda_{x_{N/2+1}}^N, \hat{u}_{1,e}^{2i-2}), \hat{u}_{2i-1}\Big), \end{aligned} \tag{9}$$

with $f(\cdot)$ and $g(\cdot)$ being

$$f(A, B) = \log\left(\frac{e^{A+B}+1}{e^A + e^B}\right), \tag{10}$$

and

$$g(A, B, c) = (-1)^c A + B, \tag{11}$$

where operator "$\oplus$" means the mod-2 sum, A, B and c are real numbers, and the recursions will continue until $L_1^{(i)} = \lambda_{x_i}$.

Benefiting from the recursively computations, the computational efficiency of soft information is improved significantly. Indeed, (11) can be further approximated as

$$f(A, B) \approx \mathrm{sign}(A) \cdot \mathrm{sign}(B) \cdot \min\{\mathrm{abs}(A), \mathrm{abs}(B)\}, \tag{12}$$

$\mathrm{sign}(\cdot)$ denotes the signum-function and $\mathrm{abs}(\cdot)$ denotes the absolute value. For convenience, we substitute $L(\lambda_{x_1}^N, \hat{u}_1^{i-1}|u_i)$ with $L(u_i)$. After the recursions, the soft output of SC decoder is the set $\mathbf{L} = \{L(u_1), L(u_2), \ldots, L(u_N)\}$. The i-th decoded bit is estimated by the hard decision according to $\mathbf{L}$, which can be described as

$$\hat{u}_i = \begin{cases} u_i, & if \quad i \in \mathcal{A}^c, \\ v_i(\lambda_{x_1}^N, \hat{u}_1^{i-1}), & if \quad i \in \mathcal{A}, \end{cases} \tag{13}$$

where

$$v_i(\lambda_{x_1}^N, \hat{u}_1^{i-1}) = \begin{cases} 0, & if \quad \mathbf{L}_i \geq 0, \\ 1, & if \quad \text{otherwise}, \end{cases} \tag{14}$$

and the decoded bits are

$$\hat{\mathbf{b}} = \{\hat{u}_i | i \in \mathcal{A}\}. \tag{15}$$

2.2 SCL Decoding

SCL decoding extends SC decoding to a more general case, where the greedy search algorithm is assisted among T decoding paths. In each path, the successive manners of SC decoding are maintained. The procedure of SCL decoding can be explained by a binary tree, the decoding algorithm searches along with T paths from the root node to the leaf nodes according to path metrics.

As shown in [12, 13, 27], the BER and BLER performances have been notably enhanced by the SCL decoding, but only at the cost of linearly increased complexity compared with SC decoding. Particularly, the LLR of i-th bit of ℓ-th path, $\ell \in T$, is formulated as

$$\begin{aligned} &L_N^{(i)}[\ell](\lambda_{x_1}^N, \hat{u}_1^{i-1}|u_i) = \\ &\qquad \log \frac{P_N^{(i)}(\lambda_{x_1}^N, \hat{u}_1^{i-1}[\ell]|u_i = 0)}{P_N^{(i)}(\lambda_{x_1}^N, \hat{u}_1^{i-1}[\ell]|u_i = 1)}. \end{aligned} \tag{16}$$

According to [27], (16) can also be calcu-

lated recursively, here we denote $L_N^{(i)}[\ell]$ short for $L_N^{(i)}[\ell](\lambda_{x_1}^N, \hat{u}_1^{i-1}[\ell]|u_i)$, then

$$L_{2N}^{(2i)}[\ell] = f(L_N^{(2i-[i \bmod \frac{N}{2}])}[\ell], L_N^{(2N+2i-[i \bmod \frac{N}{2}])}[\ell]), \tag{17}$$

and

$$L_{2N}^{(2i+1)}[\ell] = g(L_N^{(2i-[i \bmod \frac{N}{2}])}[\ell], L_N^{(2N+2i-[i \bmod \frac{N}{2}])}[\ell], u_{2N}^{(2i)}). \tag{18}$$

Meanwhile, the path metric in [27] is defined as

$$PM_\ell^{(i)} = \sum_{k=1}^{i} \log\left(1 + e^{-(1-2\hat{u}_k[\ell]\cdot L_N^{(k)}[\ell])}\right), \tag{19}$$

for effective implementation, (19) is well approximated as

$$PM_\ell^{(i)} = \begin{cases} PM_\ell^{(i-1)}, & \text{if } \hat{u}_i[\ell] = \delta\left(L_N^{(i)}[\ell]\right), \\ PM_\ell^{(i)} + \text{abs}(L_N^{(i)}[\ell]), & \text{if } \hat{u}_i[\ell] \neq \delta\left(L_N^{(i)}[\ell]\right), \\ +\infty, \text{if } x_i \text{ is frozen bit and incorrect estimated} \end{cases} \tag{20}$$

In (20), $\delta\left(L_N^{(i)}[\ell]\right)$ denotes the decision that SC decoder would take to estimate the value of u_i when $L_N^{(i)}[\ell]$ and the past i-1 estimations $\hat{u}_1^{i-1}$ are given. (20) demonstrates that the polarized sub-channels that have higher reliabilities would be assigned with smaller values of path metrics. Thus, the T decoding paths with the lowest path metrics are chosen from the binary tree in each decoding level.

Additionally, in this work, the soft information of the decoded bits $\mathbf{L}_\mathcal{A}$ is utilized not only for the estimation of bits, but also for the re-encoding of codewords.

III. PROPOSED ALGORITHM

3.1 Re-encoding

The re-encoder is the unit that calculates the soft information for polar codewords from $\mathbf{L}_\mathcal{A}$. After re-encoding, the soft information λ_{21}^N would be interleaved and be composed as symbol-level *a priori* information for the front detector. Notice that the coding structure of the polar codes is inherited by the re-encoder, hence, the essential elements of polar encoding are also necessary for polar re-encoding. By reviewing the process of polar encoding, the codewords x_1^N can be produced by multiplying u_1^N with the generator matrix G_{NN},

$$x_1^N = u_1^N G_{NN}, \tag{21}$$

where G_{NN} is an $N \times N$ matrix that can be formulated by $G_{NN} = B_N \cdot F^{\otimes t}$, where $N = 2^t$ for some $t \geq 0$, B_N is the *bit-reversal* permutation matrix and $F = \begin{bmatrix} 1 & 0 \\ 1 & 1 \end{bmatrix}$ with the operator $[\cdot]^{\otimes t}$ indicating the t-fold Kronecker power. From (21), the element x_j in x_1^N can be described as

$$x_j = u_\mathcal{A} G_{\mathcal{A}j} \oplus u_{\mathcal{A}^c} G_{\mathcal{A}^c j}, \tag{22}$$

where $G_{\mathcal{A}j}$ means the elements with the indices of $\mathcal{A}$ in the j-th column of G_{NN}. Because the frozen bits are "0", (22) can be written as

$$x_j = u_\mathcal{A} G_{\mathcal{A}j}. \tag{23}$$

Equation (23) reveales that x_j can be produced by modulo-2 sum based on $u_\mathcal{A}$. The positions of "1" in $G_{\mathcal{A}j}$ indicate which bits in $u_\mathcal{A}$ are involved in the calculation. From this perspective, there are two essential elements of polar encoding:

1) The information set, $\mathcal{A}$;

2) The indices of "1" in j-th column of G_{NN}, which is denoted as $\mathfrak{L}_j$, $\mathfrak{L}_j = \{i | G_{ij} = 1, i = 1, 2, \ldots, N\}$.

Let $\hat{x}_1^N$ be the re-encoded polar codewords, according to (23), the process of re-encoding of $\hat{x}_j$ can be written as

$$\hat{x}_j = \bigoplus_{l \in \mathfrak{L}_j} \hat{u}_l, \tag{24}$$

the big "$\bigoplus$" is the component-wise modulo-2 summation, which is

$$\bigoplus_{i=1}^{m} a_i \triangleq a_1 \oplus a_2 \oplus \cdots \oplus a_m, \tag{25}$$

based on this, the calculation of the corresponding LLR of $\hat{x}_j$ can be expressed as,

$$L\left(\hat{x}_j\right) = \log \frac{P(\hat{x}_j = 0)}{P(\hat{x}_j = 1)} = \log \frac{P\left(\bigoplus_{l\in\mathfrak{L}_j} \hat{u}_l = 0\right)}{P\left(\bigoplus_{l\in\mathfrak{L}_j} \hat{u}_l = 1\right)}. \tag{26}$$

To simplify the notations, we use $\bigoplus \hat{\mathbf{u}}_{\mathfrak{L}}$ to represent $\bigoplus_{l\in\mathfrak{L}} \hat{u}_l$. Thus, all the possible sequences of $\hat{u}_1^N$ resulting in $\bigoplus \hat{\mathbf{u}}_{\mathfrak{L}} = 0$ construct a specific vector set $\mathfrak{U}_j^{(e)}$, namely the even vector set, and its elements are denoted by $\hat{\mathbf{u}}_j^{(e)}$. Similarly, the other sequences of $\hat{u}_1^N$ resulting in $\bigoplus \hat{\mathbf{u}}_{\mathfrak{L}} = 1$ construct the vector set $\mathfrak{U}_j^{(o)}$, which is called the odd vector set, and $\hat{\mathbf{u}}_j^{(o)} \in \mathfrak{U}_j^{(o)}$. Every estimated bit $\hat{u}_l$ can be either 0 or 1. Thus, there are $2^{|\mathfrak{L}_j|-1}$ elementary sequences in both $\mathfrak{U}_j^{(e)}$ and $\mathfrak{U}_j^{(o)}$,i.e., we have

$$P\left(\bigoplus \hat{\mathbf{u}}_{\mathfrak{L}_j} = 0\right) = \sum_{\hat{\mathbf{u}}_j^{(e)}\in\mathfrak{U}_j^{(e)}} P(\hat{\mathbf{u}}_j^{(e)}), \tag{27}$$

$$P\left(\bigoplus \hat{\mathbf{u}}_{\mathfrak{L}_j} = 1\right) = \sum_{\hat{\mathbf{u}}_j^{(o)}\in\mathfrak{U}_j^{(o)}} P(\hat{\mathbf{u}}_j^{(o)}). \tag{28}$$

Depending on the polar decoding process, it holds that

$$P(\hat{\mathbf{u}}_j^{(e)}) = \prod_{i\in\mathfrak{L}_j} P_N^{(i)}(\lambda_{x_1}^N, \hat{u}_1^{i-1,(e)}|\hat{u}_i^{(e)}), \tag{29}$$

$$P(\hat{\mathbf{u}}_j^{(o)}) = \prod_{i\in\mathfrak{L}_j} P_N^{(i)}(\lambda_{x_1}^N, \hat{u}_1^{i-1,(o)}|\hat{u}_i^{(o)}), \tag{30}$$

where $\hat{u}_1^{i-1,(e)} \in \hat{\mathbf{u}}_j^{(e)}$ and $\hat{u}_1^{i-1,(o)} \in \hat{\mathbf{u}}_j^{(o)}$, $\hat{u}_i^{(e)}$ and $\hat{u}_i^{(0)}$ equal to "0" or "1". Due to the fact that the frozen bits are zero-inserted, they have no contributions to the modulo-2 summation and the values of frozen bits are foreknown for decoder, thus their associated probabilities are always 1. Accordingly, the set $\Delta_j = \mathfrak{L}_j \cap \mathcal{A}$ is further introduced, which simplifies (26) as

$$L\left(\hat{x}_j\right) = \log \frac{P\left(\bigoplus_{l\in\Delta} \hat{u}_l = 0\right)}{P\left(\bigoplus_{l\in\Delta} \hat{u}_l = 1\right)} = \log \frac{\sum_{\hat{\mathbf{u}}\in\mathfrak{U}} \left(\prod_{i\in\Delta} P_N^{(i)}(\lambda_{x_1}^N, \hat{u}_1^{i-1,(e)}|\hat{u}_i^{(e)})\right)}{\sum_{\hat{\mathbf{u}}\in\mathfrak{U}} \left(\prod_{i\in\Delta} P_N^{(i)}(\lambda_{x_1}^N, \hat{u}_1^{i-1,(o)}|\hat{u}_i^{(o)})\right)}. \tag{31}$$

Although (31) reduces the computational complexity of the re-encoding to a certain degree, it still suffers an exponential increased computational complexity of $|\Delta_j|$, which is ineffectively to be implemented for long-length codewords. Thus, (31) needs to be further simplified.

Algorithm 1. *Construction of sub-vector set.*

Input: N_f, N_p, Δ_j and $\mathbf{L}$.
Output: $\tilde{\mathfrak{U}}_j^{(e)}$ and $\tilde{\mathfrak{U}}_j^{(o)}$.
  if $|\Delta_j| \le N_f$ **then**
    $[\tilde{\mathfrak{U}}_j^{(e)}, \tilde{\mathfrak{U}}_j^{(o)}]$ = FUL(Δ_j);
  else
    $[\tilde{\mathfrak{U}}_j^{(e)}, \tilde{\mathfrak{U}}_j^{(o)}]$ = PAR($N_p, \Delta_j, \mathbf{L}$);
  end if
  return $\tilde{\mathfrak{U}}_j^{(e)}, \tilde{\mathfrak{U}}_j^{(o)}$.

3.2 The Max-re-encoder

The *max-log* algorithm reduces the computational complexity straightforwardly. However, the accuracy is degraded significantly by the *max* operations. Here, the idea of partial marginalization [28, 29] is adopted into the re-encoding, where $L\left(\hat{x}_j\right)$ is calculated depending on the parameter N_p, which means, 1) $|\Delta_j| \le N_p$, (31) is calculated completely with all $2^{|\Delta_j|}$ sequences, 2) $|\Delta_j| > N_p$, N_p sequences with highest probabilities are chosen for re-encoding. In other words, there are two sub-vector sets, $\tilde{\mathfrak{U}}_j^{(e)} \subset \mathfrak{U}_j^{(e)}$ and $\tilde{\mathfrak{U}}_j^{(o)} \subset \mathfrak{U}_j^{(o)}$, are constructed for re-encoding. The constructions of $\tilde{\mathfrak{U}}_j^{(e)}$ and $\tilde{\mathfrak{U}}_j^{(o)}$ can be realized effectively by bit flipping, thus, the *max-re-encoder* decreases the computational complexity of re-encoding from $O(2^N)$ to $O(2^{N_p})$, where $N_p \ll N$.

In more detail, the constructions of the sub-vector sets $\tilde{\mathfrak{U}}_j^{(e)}$ and $\tilde{\mathfrak{U}}_j^{(o)}$ can be realized by *Algorithm 1*.

Algorithm 2. *FUL.*

Input:Δ_j.

Output:$\tilde{\mathfrak{U}}_j^{(e)}$ and $\tilde{\mathfrak{U}}_j^{(o)}$.

$D_1^{2^{|\Delta_j|}} = [0, 1, \ldots, 2^{|\Delta_j|} - 1]^T$;

$Bs_{2^{|\Delta_j|}\times|\Delta_j|} = \textbf{de2bi}(D_1^{2^{|\Delta_j|}})$;

$Ct_1^{2^{|\Delta_j|}} = \textbf{sum}(Bs_{2^{|\Delta_j|}\times|\Delta_j|}, 2)$;

for $k = 1, 2, \ldots, 2^{|\Delta_j|}$ **do**

  if $Ct_k \bmod 2 == 1$ **then**

    $\tilde{\mathfrak{U}}_j^{(o)} \longleftarrow Bs_{2^{|\Delta_j|}\times|\Delta_j|}(k, :)$;

  else

    $\tilde{\mathfrak{U}}_j^{(e)} \longleftarrow Bs_{2^{|\Delta_j|}\times|\Delta_j|}(k, :)$;

  end if

end for

return $\tilde{\mathfrak{U}}_j^{(e)}, \tilde{\mathfrak{U}}_j^{(o)}$.

Based on $|\Delta_j|$, *Algorithm 1* is further divided into two sub-functions, $\mathsf{FUL}(\Delta_j)$ and $\mathsf{PAR}(N_p, \Delta_j, \mathbf{L})$.

$\mathsf{FUL}(\Delta_j)$ indicates the complete calculations of the re-encoding according to all possible sequences, while $\mathsf{PAR}(N_p, \Delta_j, \mathbf{L})$ indicates the partial calculations according to N_p selected sequences. Further, the minimal *Hamming* distance between $\hat{\mathbf{u}}_j^{(e)}$ and $\hat{\mathbf{u}}_j^{(o)}$ equals to 1, which means the elements of $\tilde{\mathfrak{U}}_j^{(e)}$ and $\tilde{\mathfrak{U}}_j^{(o)}$ can be produced alternately by only considering one bit flipping. Then, the flipped sequences are categorized one after another based on the parity of the initial sequence, this makes *Algorithm 3* more efficient.

The computational complexity of the *max-re-encoder* is decreased compared to (31) due to its partial calculation of the deterministic sequences. Meanwhile, the performance of the *max-re-encoder* may suffer from degradation due to its incomplete calculations of the soft information in high SNR region.

3.3 The Min-re-encoder

In order to enhance the accuracy of re-encoding, especially in high SNR region, an idea is provided by the $tanh(\cdot)$ algorithm, where $L(\hat{x}_j)$ can be computed by all involved LLRs $\mathbf{L}_{\Delta_j}$. Additionally, for the effect of random interleaver, LLRs in $\mathbf{L}_{\Delta_j}$ are relative independent. Therefore, $L(\hat{x}_j)$ can be calculated as

Algorithm 3. *PAR.*

Input: N_p, Δ_j and $\mathbf{L}$.

Output: $\tilde{\mathfrak{U}}_j^{(e)}$ and $\tilde{\mathfrak{U}}_j^{(o)}$.

$\hat{u}_1^{|\Delta_j|} = \begin{cases} 0, & if\ \ \mathbf{L}_k \geq 0, k \in \Delta_j \\ 1, & if\ \ otherwise \end{cases}$;

$\left[v_1^{|\Delta_j|}, p_1^{|\Delta_j|}\right] = \textbf{sort}(\textbf{abs}(\mathbf{L}_{\Delta_j}))$;

for $z = 1, 2, \ldots, N_p - 1$ **do**

  $\tilde{u}_1^{|\Delta_j|} = \hat{u}_1^{|\Delta_j|}$

  if $\textbf{sum}(\tilde{u}_1^{|\Delta_j|}) \bmod 2 == 1$ **then**

    $\tilde{\mathfrak{U}}_j^{(o)} \longleftarrow \tilde{u}_1^{|\Delta_j|}$;

  else

    $\tilde{\mathfrak{U}}_j^{(e)} \longleftarrow \tilde{u}_1^{|\Delta_j|}$;

  end if

  $\hat{u}_1^{|\Delta_j|} = \textbf{flip}(\tilde{u}_1^{|\Delta_j|}, p_z)$;

end for

return $\tilde{\mathfrak{U}}_j^{(e)}, \tilde{\mathfrak{U}}_j^{(o)}$;

$$
\begin{aligned}
L(\hat{x}_j) &= L_R\left(\bigoplus_{l\in\Delta}\hat{u}_l\right) \\
&= \log\frac{\prod_{l\in\Delta}\left(e^{\mathbf{L}}+1\right)+\prod_{l\in\Delta}\left(e^{\mathbf{L}}-1\right)}{\prod_{l\in\Delta}\left(e^{\mathbf{L}}+1\right)-\prod_{l\in\Delta}\left(e^{\mathbf{L}}-1\right)} \\
&= \log\frac{1+\prod_{l\in\Delta}\tanh(\mathbf{L}_l/2)}{1-\prod_{l\in\Delta}\tanh(\mathbf{L}_l/2)},
\end{aligned}
\tag{32}
$$

then (32) can also be approximated as

$$
\begin{aligned}
L(\hat{x}_j) &= 2\text{arctanh}\left(\prod_{l\in\Delta_j}\tanh(\mathbf{L}_l/2)\right) \\
&\approx \left(\prod_{l\in\Delta_j} sign(\mathbf{L}_l)\right)\cdot \min_{l\in\Delta_j}\{abs(\mathbf{L}_l)\}.
\end{aligned}
\tag{33}
$$

This algorithm is named the *min-re-encoder*, which is similar to the min-sum algorithm that has been implemented for LDPC decoding.

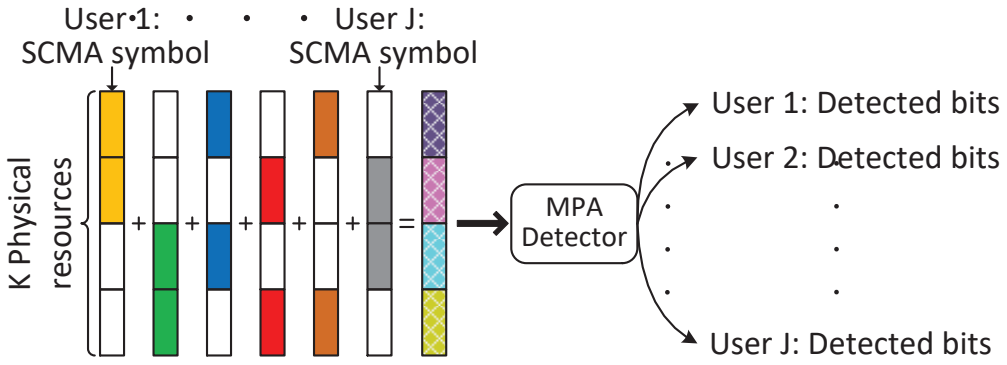

Figure 3. *The principle of SCMA.*

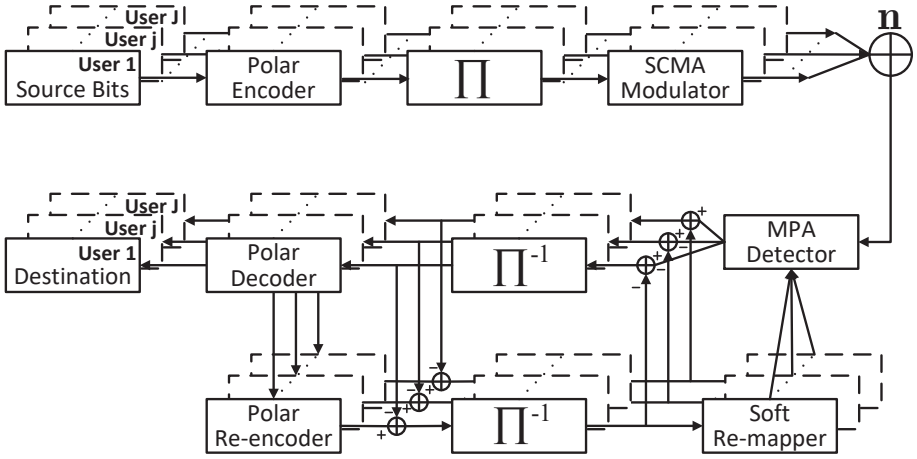

Figure 4. *The multi-user system.*

3.4 Re-mapping

After re-encoding, the extrinsic information λ_2 is interleaved as $\tilde{\lambda}_c = \Pi(\lambda_2)$. Then, $\tilde{\lambda}_c$ are re-mapped to symbol-level probabilities $\mathbf{P_s}$ for updating the *priori* information. For the k-th re-mapped symbol $\hat{s}_k$, the probability can be written as

$$\begin{aligned}\mathbf{P_s}(\hat{s}_k) &= \prod_{i=m(k-1)+1}^{mk} P(\hat{c}_i) \\ &= \prod_{i=m(k-1)+1}^{mk} \hat{c}_i \tanh\left(\frac{\tilde{\lambda}_{c_i}}{2}\right) + \Psi(\tilde{\lambda}_{c_i}),\end{aligned} \tag{34}$$

where, $\Psi(\tilde{\lambda}_{c_i}) = e^{\tilde{\lambda}_{c_i}}/(1+e^{\tilde{\lambda}_{c_i}})$, $k = 1, 2, \ldots, N_s$, $\hat{c}_i \in \{0, 1\}$ is the estimated bit according to the LLR $\tilde{\lambda}_{c_i}$. One iteration is considered to be completed when the re-mapped symbol-level information is fed into the detector. The iterative decoding will continue until the maximum number of iteration I_{BICM} is reached.

IV. MULTI-USER SCENARIO

4.1 SCMA

In this work, SCMA is employed to provide the multi-user access [30]. The high overload ratio and massive connectivity make SCMA be a potential multiplexing technique for the future mobile networks, especially for the mMTC. The principle of SCMA is depicted in figure 3.

At the transmitter, the information bits are modulated to the short spread SCMA symbol according to user's unique codebook. Then, the modulated symbols of all users are overlapped in the physical resources. Note that, the physical resources can be frequency carriers and time slots. At the receiver, information bits of each user are detected by the MPA detector. By taking advantage of the sparsity, the complexity of

MPA detection is reduced significantly from the optimal scheme, while with similar accuracy. Then, combining the BIPCM-ID with SCMA, an unlink multi-user system is depicted in figure 4.

As can be observed from figure 4, the transmitter and the receiver of each user are identical with the single-user, except for the modulator and the demodulator. In multi-user scenario, the QAM constellations and the MAP detector are replaced by the multi-dimensional SCMA constellations and the MPA detector accordingly. Here, the physical resources are the frequency carriers, while perfect synchronization is assumed in overlapping. Thus, the received signals in a time slot can be expressed as

$$\mathbf{y} = \sum_{j=1}^{J} \mathrm{diag}(\mathbf{h}[j])\mathbf{s}[j] + \mathbf{n}, \tag{35}$$

where, $\mathbf{n}$ is a $K \times 1$ vector representing the complex AWGN vector with zero mean and $N_0\mathbf{I}$ variance, $\mathbf{I}$ is identity matrix, $\mathbf{s}[j]$ is the SCMA codebook of user j, $\mathbf{s}[j] = (s_1[j], s_2[j], \ldots, s_K[j])^T$, $\mathbf{h}[j] = (h_1[j], h_2[j], \ldots, h_K[j])^T$.

4.2 Effects on Average Mutual Information

The channel splitting of polar code is based on the splitting of the synthesized channel vector into the N binary-input sub-channels, which is defined by the channel transition probability

$$P_N^{(i)}(y_1^N, u_1^{(i-1)}|u_i) = \sum_{u_{i+1}^N \in \mathbb{B}^{N-i}} \frac{1}{2^{N-1}} P_N(y_1^N|u_1^N), \tag{36}$$

where $\mathbb{B} = \{0, 1\}$ represents the binary-input alphabet. Here, we denote the corresponded MI of the i-th sub-channel $\mathsf{I}(W_N^{(i)})$ as $\mathsf{I}_N^{(i)}$.

The proposed BIPCM-ID further polarizes the MI of sub-channels into 0 or 1, which is shown in figure 5. By employing the re-encoder, the values of MI of sub-channels are divided much more, which means the number of sub-channels that $\mathsf{I}_N^{(i)} \in [0.2, 0.8]$, $i = 1, 2, \ldots, N$ decreases from dozens to sporadic, and their values are accumulated within some MI layers, such as $\mathsf{I}_N = 0.9$ and $\mathsf{I}_N = 0.12$ after 3-times re-encoding.

The capacity of a coded modulation system is defined as the AMI between the transmitted and decoded symbols, where $\mathbf{s} \in \mathbf{S}$ and $\mathbf{y} \in \mathbf{Y}$, $\mathbf{S}$ and $\mathbf{Y}$ are the alphabets of the transmitted symbols and the received signals for multi-user that have been overlapped in the wireless space, thus,

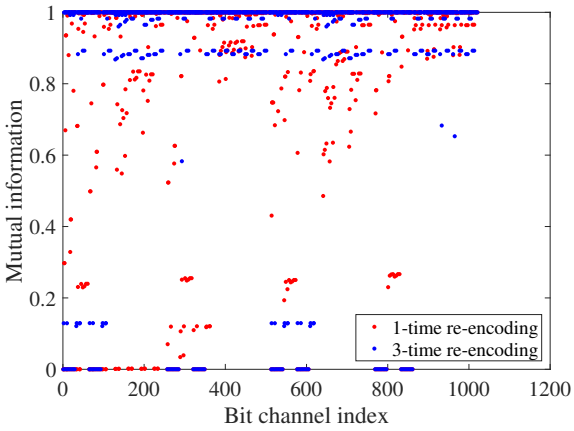

Figure 5. *The mutual information of sub-channels after the re-encoding for $N = 1024$, $Eb/No = 1.9$ and $R = 0.5$.*

$$\begin{aligned} \mathsf{I}_{\mathbf{S}}(\mathbf{S};\mathbf{Y}) &= \mathbb{E}_{\mathbf{S},\mathbf{Y}}\left[\log_2 \frac{P_{\mathbf{S},\mathbf{Y}}(\mathbf{s},\mathbf{y})}{P_{\mathbf{S}}(\mathbf{s})P_{\mathbf{Y}}(\mathbf{y})}\right] \\ &= \mathbb{E}_{\mathbf{S},\mathbf{Y}}\left[\log_2 \frac{P_{\mathbf{Y}|\mathbf{S}}(\mathbf{y}|\mathbf{s})}{P_{\mathbf{Y}}(\mathbf{y})}\right], \end{aligned} \tag{37}$$

according to the proposed multi-user system, the AMI of the t-th iteration can be written as

$$\begin{aligned} \mathsf{I}_{\mathbf{S}}^t(\mathbf{S};\mathbf{Y}) = \frac{1}{J}\sum_{j=1}^{J}\sum_{q=1}^{m'}\sum_{b\in\mathbb{B}}\sum_{i\in\mathcal{I}_{q,b}} \\ P_{\mathbf{s}[j]}^{t-1}(\mathbf{s}[j]_i)\cdot\int_{\mathcal{D}} P_{\mathbf{Y}|\mathbf{s}[j]}^t(\mathbf{y}|\mathbf{s}[j]_i) \\ \cdot\log_2\frac{\sum_{l\in\mathcal{I}_{q,b}} P_{\mathbf{s}[j]|c_q=b}^t(\mathbf{s}[j]_l|b)P_{\mathbf{Y}|\mathbf{s}[j]}^t(\mathbf{y}|\mathbf{s}[j]_l)}{\sum_{\mathbf{s}[j]_l\in\mathbf{s}[j]} P_{\mathbf{s}[j]}^{t-1}(\mathbf{s}[j]_l)P_{\mathbf{Y}|\mathbf{s}[j]}^t(\mathbf{y}|\mathbf{s}[j]_l)} d\mathbf{y}, \end{aligned} \tag{38}$$

where $\mathcal{D}$ is the K-dimensional complex domain for $\mathbf{y}$, $\mathcal{I}_{q,b}$ is the set of indices of the symbols with a binary label $b \in \mathbb{B}$ at bit position $q = 1, 2, \ldots, m'$, $m' = \log_2|\mathbf{s}[j]|$. In (38), $\mathbf{s}[j]_i$ denotes the i-th K-dimensional constellation point of $\mathbf{s}[j]$. In this system, the *a posteriori* information is calculated by the MPA

detector, thus (38) can be rewritten as

$$\mathrm{I}_{\mathbf{S}}^{t}(\mathbf{S};\mathbf{Y}) \approx \frac{1}{J}\sum_{j=1}^{J}\sum_{q=1}^{m'}\sum_{b\in\mathbb{B}}\sum_{i\in\mathcal{I}_{q,b}} P_{\mathbf{s}[j]}^{t-1}(\mathbf{s}[j]_i) \cdot \int_{\mathcal{D}} Q(\mathbf{y},\mathbf{s}[j]_i)\log_2 \frac{\sum_{l\in\mathcal{I}_{q,b}} Q(\mathbf{y},\mathbf{s}[j]_l)}{\sum_{\mathbf{s}[j]_l\in\mathbf{s}[j]} P_{\mathbf{s}[j]}^{t-1}(\mathbf{s}[j]_l)Q(\mathbf{y},\mathbf{s}[j]_l)} d\mathbf{y}, \tag{39}$$

In more detail, $Q(\mathbf{y},\mathbf{s}[j]_i)$ indicates the process of MPA detection that without outputting of estimations, which can be expressed as

$$Q(\mathbf{y},\mathbf{s}[j]_i) = \prod_{k\in\varphi_j} R_{k\to j}^{I_{\mathrm{MPA}}}(\mathbf{s}[j]_i), \tag{40}$$

where, I_{MPA} is the maximum number of inner iteration of the MPA detector. The messages that are passed between j-th variable node and k-th source node are

$$R_{k\to j}^{t}(\mathbf{s}[j]_i) = \sum_{\mathbf{s}[\hat{j}]:\hat{j}\in\phi/j} P(y_k|\mathbf{s}[j]_i)\prod_{\hat{j}\in\phi/j} R_{\hat{j}\to k}^{t-1}(\mathbf{s}[\hat{j}]_i), \tag{41}$$

$$R_{j\to k}^{t}(\mathbf{s}[j]_i) = \prod_{\hat{k}\in\varphi_j/k} R_{\hat{k}\to j}^{t}(\mathbf{s}[j]_i), \tag{42}$$

where, $R_{\mathbf{s}[j]}^{0}(\mathbf{s}[j]_i) = 1/|\mathbf{s}[j]|$, $\phi_k = \{j : 1 \le j \le J, \mathbf{F}_{kj} \ne 0\}$, $\varphi_j = \{k : 1 \le k \le K, \mathbf{F}_{kj} \ne 0\}$. $\mathbf{F}_{K\times J}$ is the factor graph matrix of SCMA and the *posteriori* probability in (35a) is

$$P(y_k|\mathbf{s}[j]_i) = \frac{1}{\pi N_0}\exp\left(-\frac{1}{N_0}\|y_k - \sum_{j\in\phi_k} h_k[j]s_k[j]_i\|^2\right). \tag{43}$$

(39) shows that the AMI of the t-th iteration is mainly affected by the updated symbol-level *priori* information calculated from the previous iteration. The calculation of updated symbol-level *priori* information is shown in (34).

V. SIMULATIONS AND DISCUSSIONS

5.1 AMI

The AMI performances of polar and LDPC codes are shown in figure 6, where the *Shannon bound* (the capacity of an AWGN channel with complex Gaussian input) is presented as benchmark. As can be observed, when $I_{\mathrm{BICM}} = 1$, the AMI of both polar and LDPC codes are almost the same, which are dominated by the wireless channel at this point. When $I_{\mathrm{BICM}} > 1$, due to the deterministic probabilities of the frozen bits in polar codewords, the corresponding AMI is increased dramatically, and the AMI of LDPC codes also increases sharply when E_b/N_o becoming larger. Then, the AMI of these two codes achieve the upper bound when E_b/N_o is large enough, such as $E_b/N_o = 10dB$.

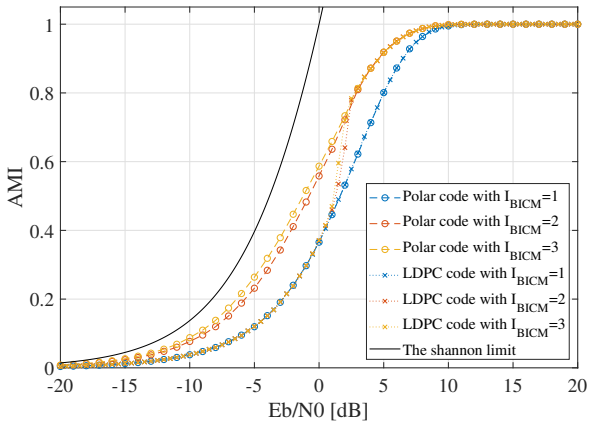

Figure 6. *The AMI performances of polar code and LDPC code.*

Comparing the different codes in terms of capacity-approaching capability, it is noted that the gaps of AMI between these two codes and the *Shannon bound* are mainly resulted from the finite code length. In this system, the lengths of polar and LDPC codewords are configured with 1024 and 1296 respectively. However, it also observed that the AMI of polar codes are able of approaching the *Shannon bound*, even closer than LDPC codes when $E_b/N_o < 2dB$.

5.2 Single-user Scenario

In this subsection, simulations are carried out based on the system depicted in figure 1 and figure 2. BER and BLER performances are shown in figure 7 and figure 8. In both figures, the polar codewords are modulated by QPSK at the transmitter, note that, the "Anti-Gray" labeled QPSK is employed in purpose of obtaining the iterative gain. Then, the modulated symbols are transmitted through an AWGN channel. In order to investigate how BER and BLER performances influ-

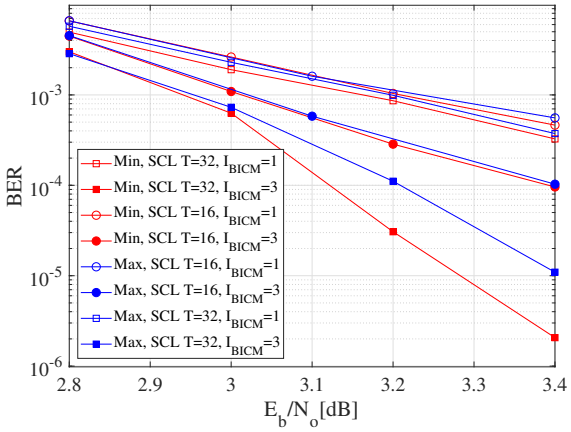

Figure 7. *The BER performance of iterative receiver of polar coded QPSK system for single user.*

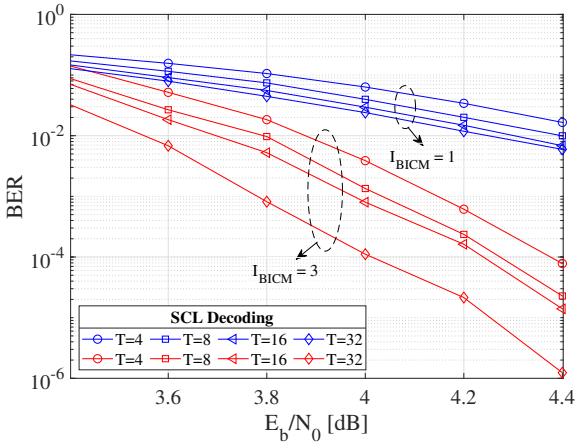

Figure 9. *The BER performances of proposed BIPCM-ID system associating with SCMA.*

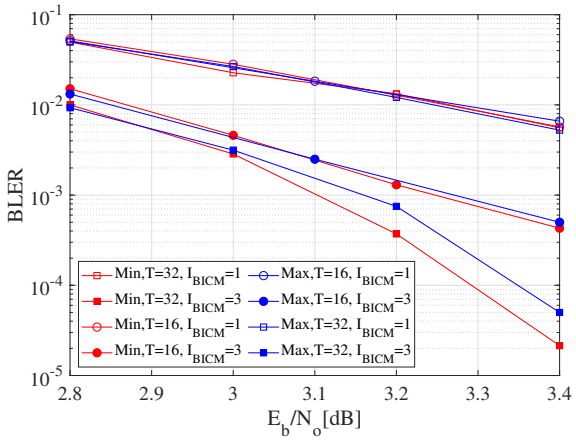

Figure 8. *The BLER performance of iterative receiver of polar coded QPSK system for single user.*

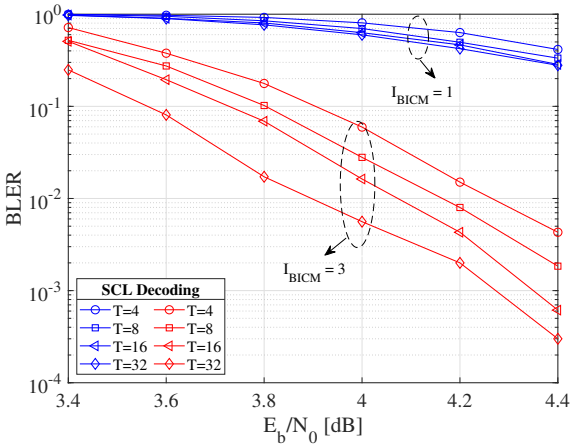

Figure 10. *The BLER performances of proposed BIPCM-ID system associating with SCMA.*

enced by the *max-re-encoder* and the *min-re-encoder*, the link-level system is configured with identical functional units and parameters except for the re-encoder. The block length of polar codes is $N = 1024$ and code rate is $R = 0.5$, at the receiver, SCL decoder is employed.

Figure 7 represents the BER and BLER performances of the *max-re-encoder* and the *min-re-encoder* respectively. As one can observe, the BER and BLER performances of polar codes are significantly improved by the proposed BIPCM-ID strategy for single-user. In general, the performances of the *min-re-encoder* are better than the *max-re-encoder*. However, when the system configured with less iterations or less SCL decoding paths, the difference of performances between these two re-encoders is minor. For example, the *min-re-encoder* holds only 0.1dB superiority at the target BER 1×10^{-5} when $I_{\mathrm{BICM}} = 3$. Correspondingly, in the performances of BLER, the difference between these two re-encoders is further reduced to 0.05dB when the BLER arriving at 1×10^{-4}.

5.3 Multi-user Scenario

In this subsection, we investigate the performances of the proposed BIPCM-ID in multi-user scenario, where only the *min-re-encoder* is employed for reducing the complexity. The multi-user accessing is provided by SCMA, the details of transmitting and receiving techniques of SCMA are explicitly demonstrated in [31–34].

5.3.1 Configuration of SCMA

In simulations, the SCMA system is configured with $K = 4$ and $J = 6$, which realizes a overloading of 150%, and every m bits are mapped into a K-dimensional symbol via each user's unique codebook. At the receiver, the MPA is used for multi-user detection. Here, we set the inner iteration of MPA detector as $I_{\mathrm{MPA}} = 3$ and the outer iteration $I_{\mathrm{BICM}} = 3$ as well. Note that, when $I_{\mathrm{BICM}} = 1$, all constellation points are equiprobable. While $I_{\mathrm{BICM}} > 1$, the *priori* information of the MPA detector will be updated by the probabilities that calculated from the re-encoded LLRs. In addition, the factor graph matrix is

$$\mathbf{F}_{4\times 6} = \begin{pmatrix} 1 & 0 & 1 & 0 & 1 & 0 \\ 0 & 1 & 1 & 0 & 0 & 1 \\ 1 & 0 & 0 & 1 & 0 & 1 \\ 0 & 1 & 0 & 1 & 1 & 0 \end{pmatrix}.$$

5.3.2 BER and BLER

It can be observed in figure 9 and figure 10, in the multi-user scenario, it's very hard to obtain acceptable performance by only detecting and decoding once, even the SCL decoder is configured with a preferable parameter, $T = 32$. While associated with the re-encoder, the BIPCM-ID is enabled of attaining remarkable performances improvements. When $I_{\mathrm{BICM}} > 1$, the re-encoder yields out the soft information of every codeword with much higher accuracy than that firstly detected from the MPA detector. Meanwhile, the re-encoder is also strongly influenced by the accuracy of its input, which means the larger T of SCL decoder results in the higher quality of re-encoding, and such advantage will be extended during iterations. This phenomenon is more obvious in BER performance.

The improvements obtained by the proposed BIPCM-ID are similar to the cyclic redundancy check aided SCL (Ca-SCL) decoding [35], but with less system overhead. It mainly resulted from the fact that the Ca-SCL replaces dozens of information bits by CRC bits, and the CRC checking processes are sequentially implemented along with T decoding paths. In this phase, the proposed BIPCM-ID may be more appropriate for the mMTC that extremely short-length codewords (dozens bits) are utilized.

Additionally, with the aid of the re-encoder, it makes the proposed BIPCM-ID system capable of challenging some classical BICM-ID systems in multi-user scenario. The BER comparisons of polar, LDPC and Turbo codes are presented in figure 11, while the simulation result of the min-sum BP (MSBP) decoded BIPCM-ID is also presented. In the simulation, it has been assumed that the *min-re-encoder* is equipped for SCL decoding, and all the codes are configured with $R = 0.5$ and $N = 1024$, except for the 1296-bit of LDPC codes. According to figure 11, the proposed BIPCM-ID has almost 1dB gain over the MSBP decoded BIPCM-ID when BER is around at 1×10^{-4}. Meanwhile, the proposed BIPCM-ID system has superior performance compared with LDPC-BICM-ID and Turbo-BICM-ID systems.

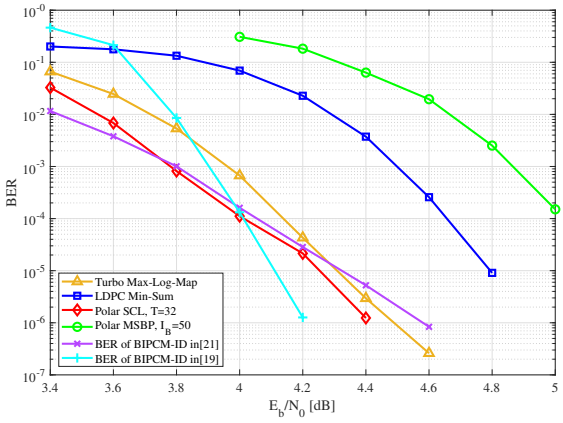

Figure 11. *The BER comparison between various BICM-ID schemes.*

In [19] and [21], BP and SCAN decoder are used respectively. In the simulation, their inner iterations are $I_{BP} = 50$ and $I_{SCAN} = 50$, and both of them are used in the BIPCM-ID system with $I_{BICM} = 3$. As can be observed in figure 11, the performance of the method proposed in [19] is excellent, especially when $E_b/N_0 > 4dB$, the BER decreases very fast with the increasing of E_b/N_0. However the computational complexity of [19] is much higher than our proposed strategy, due to the employment of BP decoder. The performance of the method proposed in [21] is very close to our curve, but we still have almost 0.2dB gain when BER is 1×10^{-6} .

5.4 Computational Complexity

Decoding complexity plays a significant role in the design of practical communication systems [36–38]. In

Table 1. *The computational complexities of basic operators of iterative successive cancellation list decoder, min-sum decoder and max-log-map decoder.*

Decoder	Polar:SCL			LDPC:min-sum		Turbo:max-log-map
	Decoding	Max re-encoder	Min re-encoder	Check node	Variable node	-
"+"	$T\log_2 N$	$2\lvert\tilde{\mathfrak{U}}_j\rvert-2$	-	$d_c+\lceil\log_2 d_c\rceil-2$	d_v-1	$10\times 2^M+11$
"×"	$T\log_2 N$	$2\lvert\Delta_j\rvert-1$	$\lvert\Delta_j\rvert$	d_c-1	-	8
Special opts.	-	-	$\lvert\Delta_j\rvert*\tanh+\tanh^{-1}$	-	-	$(5\times 2^M-2)*\max$
Notations list	◇ The computational complexity of SC decoding for j-th bit refers to an average decoding computational complexity of a polar code with length N. ◇ d_c and d_v are the check degree and variable degree of the j-th LDPC code, respectively. ◇ M is the memory length of the component code of the Turbo code.					

this subsection, the numbers of execution of the basic operators of polar, LDPC and Turbo decoders are counted in one iteration. For example, the additions and multiplications.

In more detail, the min-sum decoder of LDPC codes is set with $I_{\mathrm{L}}=50$ inner iterations. For Turbo codes, the memory length of the component encoder is $M=4$ and the encoding coefficient is $\{11,13\}$, the inner iterations of the max-log-map decoder is $I_{\mathrm{T}}=2$. For polar codes, 1) the basic operator of MSBP decoder is the processing element (PE), thus, the decoding of a length-N polar codeword needs $\log_2(N^2/2)$ PEs, which work stage by stage, and the messages are passed from left to right and right to left according to the factor graph. The inner iterations of MSBP is $I_{\mathrm{BP}}=60$; 2) due to the SCL decoder and the re-encoder are two independent units, the computational complexity of these two units can be calculated separately, and the total computational complexity is the summation of these two units.

It is worth noting that, the computational complexity of the re-encoder will not be affected by the SCL decoder, which means the computational complexity of SCL decoder increases linearly in terms of the list size T, while the re-encoder only cares about the length of codeword N.

The computational complexity of the basic operators of different codes are presented in TABLE 1, and the total computational complexity in one iteration of these considered decoders are shown in figure 12, in which the *max-re-encoder* and the *min-re-encoder* are denoted as A.1 and A.2.

It can be observed from figure 12, the MSBP decoder has the highest computational complexity, although it has been further reduced by the min-sum algorithm. This is due to the large numbers of inner iterations, which is similar with the LDPC min-sum decoder. The high computational complexity of max-log-map decoder of Turbo codes mainly resulted from the large numbers of max operations. The proposed iterative SCL decoder maintains the low computational complexity even the list size $T=32$. At the same time, the computational complexity of re-encoder is acceptable, especially when the *min-re-encoder* is employed.

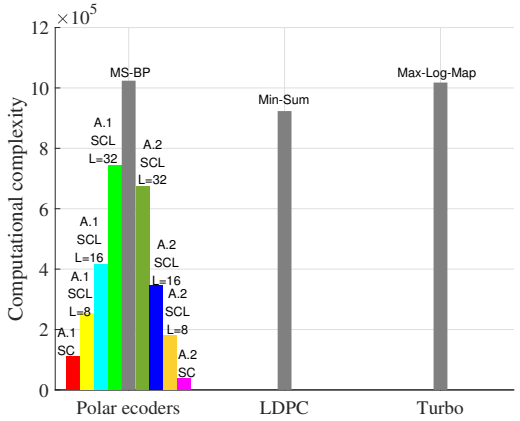

Figure 12. *The comparison of computational complexity between different decoders.*

VI. CONCLUSION

In this paper, we provide the BIPCM-ID by invoking a SISO polar decoder, which is a novel scheme of improving the performance of polar coded modulation. The iterative decoding enabled by the re-encoder further polarized the MI of sub-channels, which is helpful of attaining the coding gain. Meanwhile, the AMI of the multi-user system is verified to approach the *Shannon bound* under the given configurations. Finally, BER and BLER according to single-user and multi-user are investigated. The simulation results show that the proposed BIPCM-ID can achieve better

performance compared with LDPC/Turbo-BICM-ID, at the expense of acceptable computational complexity. Therefore, it can be concluded that the proposed scheme for the BIPCM-ID is practical and effective, especially for the multi-user scenario with short frame length.

References

[1] E. Arikan, "Channel polarization: A method for constructing capacity-achieving codes for symmetric binary-input memoryless channels," *IEEE Transactions on information Theory*, vol. 55, no. 7, 2009, pp. 3051–3073.

[2] M. Seidl, A. Schenk, *et al.*, "Polar-coded modulation," *IEEE Transactions on Communications*, vol. 61, no. 10, 2013, pp. 4108–4119.

[3] X. Wu and Z. Wu, "Performance analysis of scma system based on polar codes," in *2018 IEEE Globecom Workshops (GC Wkshps)*. IEEE, 2018, pp. 1–5.

[4] S. Jing, C. Yang, *et al.*, "Joint detection and decoding of polar-coded scma systems," in *2017 9th International Conference on Wireless Communications and Signal Processing (WCSP)*. IEEE, 2017, pp. 1–6.

[5] Z. Ma, Z. Zhang, *et al.*, "Key techniques for 5g wireless communications: network architecture, physical layer, and mac layer perspectives," *Science China information sciences*, vol. 58, no. 4, 2015, pp. 1–20.

[6] E. Zehavi, "8-psk trellis codes for a rayleigh channel," *IEEE Transactions on Communications*, vol. 40, no. 5, 1992, pp. 873–884.

[7] G. Caire, G. Taricco, *et al.*, "Bit-interleaved coded modulation," *IEEE transactions on information theory*, vol. 44, no. 3, 1998, pp. 927–946.

[8] X. Li and J. A. Ritcey, "Bit-interleaved coded modulation with iterative decoding using soft feedback," *Electronics Letters*, vol. 34, no. 10, 1998, pp. 942–943.

[9] D.-M. Shin, S.-C. Lim, *et al.*, "Mapping selection and code construction for 2ˆ m-ary polar-coded modulation," *IEEE Communications Letters*, vol. 16, no. 6, 2012, pp. 905–908.

[10] K. Chen, K. Niu, *et al.*, "An efficient design of bit-interleaved polar coded modulation," in *2013 IEEE 24th Annual International Symposium on Personal, Indoor, and Mobile Radio Communications (PIMRC)*. IEEE, 2013, pp. 693–697.

[11] H. Mahdavifar, M. El-Khamy, *et al.*, "Polar coding for bit-interleaved coded modulation," *IEEE Transactions on Vehicular Technology*, vol. 65, no. 5, 2015, pp. 3115–3127.

[12] S. A. Hashemi, C. Condo, *et al.*, "Fast and flexible successive-cancellation list decoders for polar codes," *IEEE Transactions on Signal Processing*, vol. 65, no. 21, 2017, pp. 5756–5769.

[13] I. Tal and A. Vardy, "List decoding of polar codes," *IEEE Transactions on Information Theory*, vol. 61, no. 5, 2015, pp. 2213–2226.

[14] E. Arıkan, "Polar codes: A pipelined implementation," *Proc. 4th ISBC*, 2010, pp. 11–14.

[15] J. Guo, M. Qin, *et al.*, "Enhanced belief propagation decoding of polar codes through concatenation," in *2014 IEEE International Symposium on Information Theory*. IEEE, 2014, pp. 2987–2991.

[16] Y. Zhang, A. Liu, *et al.*, "A modified belief propagation polar decoder," *IEEE communications letters*, vol. 18, no. 7, 2014, pp. 1091–1094.

[17] U. U. Fayyaz and J. R. Barry, "Low-complexity soft-output decoding of polar codes," *IEEE Journal on Selected Areas in Communications*, vol. 32, no. 5, 2014, pp. 958–966.

[18] Q. Zhang, A. Liu, *et al.*, "Practical design and decoding of parallel concatenated structure for systematic polar codes," *IEEE Transactions on Communications*, vol. 64, no. 2, 2015, pp. 456–466.

[19] S. Saha, M. Tschauner, *et al.*, "Bit-interleaved polar coded modulation with iterative decoding," in *2018 International Conference on Military Communications and Information Systems (ICMCIS)*. IEEE, 2018, pp. 1–8.

[20] F. Cheng, A. Liu, *et al.*, "Codes design based on exit chart for polar coded bicm-id," in *2017 IEEE 2nd Advanced Information Technology, Electronic and Automation Control Conference (IAEAC)*. IEEE, 2017, pp. 1129–1133.

[21] U. U. Fayyaz, "Symbol mapping design for bit-interleaved polar-coded modulation with iterative decoding," *IEEE Communications Letters*, vol. 23, no. 1, 2018, pp. 32–35.

[22] T. Wang, D. Qu, *et al.*, "Parity-check-concatenated polar codes," *IEEE Communications Letters*, vol. 20, no. 12, 2016, pp. 2342–2345.

[23] J. Dai, K. Niu, *et al.*, "Polar-coded non-orthogonal multiple access," *IEEE Transactions on Signal Processing*, vol. 66, no. 5, 2017, pp. 1374–1389.

[24] J. Tong, H. Zhang, *et al.*, "A soft cancellation decoder for parity-check polar codes," in *2020 IEEE 31st Annual International Symposium on Personal, Indoor and Mobile Radio Communications*. IEEE, 2020, pp. 1–6.

[25] M. Geiselhart, A. Elkelesh, *et al.*, "Crc-aided belief propagation list decoding of polar codes," in *2020 IEEE International Symposium on Information Theory (ISIT)*. IEEE, 2020, pp. 395–400.

[26] L. Xiang, Y. Liu, *et al.*, "Soft list decoding of polar codes," *IEEE Transactions on Vehicular Technology*, vol. 69, no. 11, 2020, pp. 13 921–13 926.

[27] A. Balatsoukas-Stimming, M. B. Parizi, *et al.*, "Llr-based successive cancellation list decoding of polar codes," *IEEE transactions on signal processing*, vol. 63, no. 19, 2015, pp. 5165–5179.

[28] E. G. Larsson and J. Jalden, "Fixed-complexity soft mimo detection via partial marginalization," *IEEE transactions on Signal Processing*, vol. 56, no. 8, 2008, pp. 3397–3407.

[29] D. Persson and E. G. Larsson, "Partial marginalization soft mimo detection with higher order constellations," *IEEE Transactions on Signal Processing*, vol. 59, no. 1, 2010, pp. 453–458.

[30] H. Nikopour and H. Baligh, "Sparse code multiple access," in *2013 IEEE 24th Annual International Symposium on Personal, Indoor, and Mobile Radio Communications (PIMRC)*. IEEE, 2013, pp. 332–336.

[31] J. Bao, Z. Ma, *et al.*, "On the design of multiuser codebooks for uplink scma systems," *IEEE Communications Letters*, vol. 20, no. 10, 2016, pp. 1920–1923.

[32] H. Mu, Z. Ma, *et al.*, "A fixed low complexity message pass algorithm detector for up-link scma system," *IEEE Wireless*

Communications Letters, vol. 4, no. 6, 2015, pp. 585–588.
[33] K. Au, L. Zhang, *et al.*, "Uplink contention based scma for 5g radio access," in *2014 IEEE Globecom workshops (GC wkshps)*. IEEE, 2014, pp. 900–905.
[34] H. Nikopour, E. Yi, *et al.*, "Scma for downlink multiple access of 5g wireless networks," in *2014 IEEE global communications conference*. IEEE, 2014, pp. 3940–3945.
[35] K. Niu and K. Chen, "Crc-aided decoding of polar codes," *IEEE communications letters*, vol. 16, no. 10, 2012, pp. 1668–1671.
[36] K. Niu, K. Chen, *et al.*, "Polar codes: Primary concepts and practical decoding algorithms," *IEEE Communications magazine*, vol. 52, no. 7, 2014, pp. 192–203.
[37] P.-Y. Wu, "On the complexity of turbo decoding algorithms," in *IEEE VTS 53rd Vehicular Technology Conference, Spring 2001. Proceedings (Cat. No. 01CH37202)*, vol. 2. IEEE, 2001, pp. 1439–1443.
[38] J. Chen, A. Dholakia, *et al.*, "Reduced-complexity decoding of ldpc codes," *IEEE transactions on communications*, vol. 53, no. 8, 2005, pp. 1288–1299.

Biographies

Hang Mu received his Ph.D. degree in information and communication engineering from the Southwest JiaoTong University in June 2019. He is currently an engineer with the 10th Research Institute of China Electronic Technology Group Corporation, Chengdu, China. His research interests include information and coding theory, machine learning and digital signal processing.

Zheng Ma is a senior member IEEE. He received the B.S. and Ph.D. degrees in communications and information system in 2000 and 2006 respectively from Southwest Jiaotong University. He is currently a professor in Southwest Jiaotong University, and servers as deputy dean of school of information science and technology. Dr Ma's research interests include: information theory & coding, signal design & applications, FPGA/DSP Implementation, and professional mobile radio (PMR).

George K. Karagiannidis is Fellow IEEE. He received the University Diploma (5 years) and Ph.D. degree, both in electrical and computer engineering from the University of Patras, in 1987 and 1999, respectively. In June 2004, he joined the faculty of Aristotle University of Thessaloniki, Greece, where he is currently Professor with the Electrical & Computer Engineering Dept. and Head of Wireless Communications & Information Processing (WCIP) Group. His research interests are in the broad area of digital communications systems and signal processing.

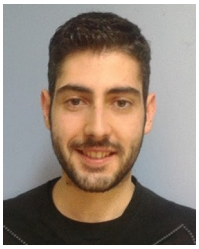

Panagiotis D. Diamantoulakis is a senior member IEEE. He received the Diploma (five years) and Ph.D. degrees from the Department of Electrical and Computer Engineering, Aristotle University of Thessaloniki (AUTH), Greece, in 2012 and 2017, respectively. Since 2017, he has been a post-doctoral fellow with the Wireless Communications Systems Group (WCSG), AUTH. His current research interests include resource allocation in optical wireless communications, nonorthogonal multiple access, and wireless power transfer.